CF_4 Plasma Functionalized Polypropylene Separator for Dendrite-Free Lithium Metal Anodes

Shengling Cao [a, b], Xin He [a], Manlin Chen [b], Yu Han [b], Kangli Wang [a], Kai Jiang [a], Min Zhou * [a]

a State Key Laboratory of Advanced Electromagnetic Engineering and Technology, School of Electrical and Electronic Engineering, Huazhong University of Science and Technology, Wuhan, China

b State Key Laboratory of Materials Processing and Die & Mould Technology, School of Materials Science and Engineering, Huazhong University of Science and Technology, Wuhan, China

The corresponding author,

E-Mail Address: minzhou0729@hust.edu.cn (M. Zhou)

1. CF_4 Plasma Emission Spectrum

The peaks of active F, C, and Fe atoms and CF_2, C_2 groups are visible in the OES spectra of CF_4 plasma and CF_4 plasma treatment on Polypropylene separator. F and C are produced during the breakdown of CF_4, and Fe is produced by the stainless steel tube wall. The fact that both spectra are nearly identical shows that the environment is unaffected by the introduction of the PP separator.

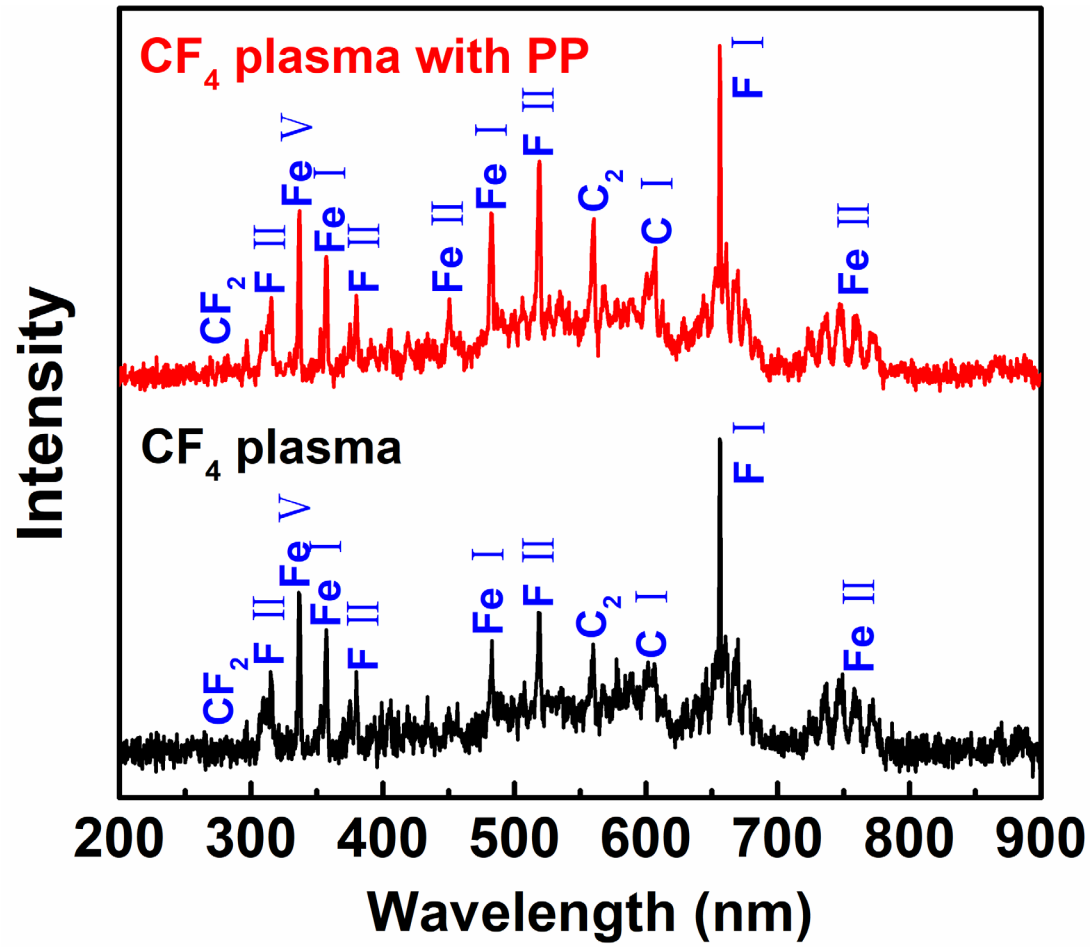

Fig. S1. CF_4 plasma Emission Spectrum

2. SEM Images

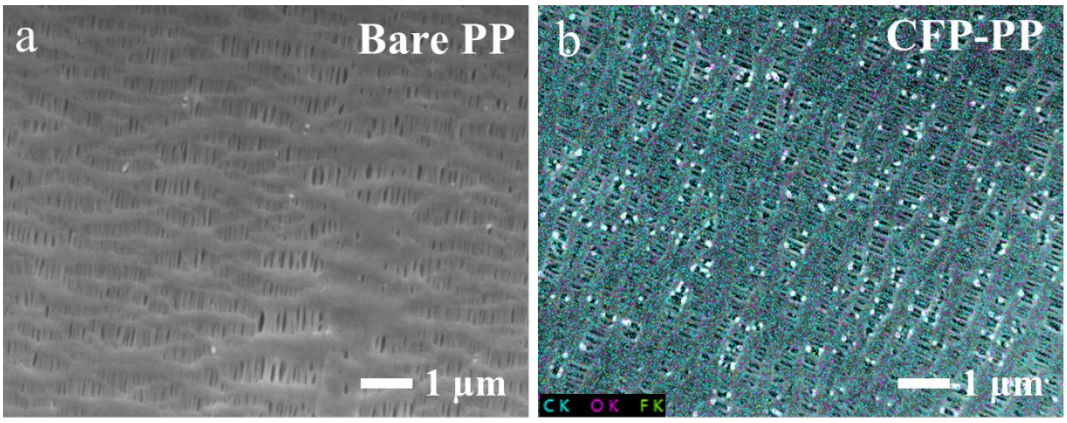

Fig. S2. a) SEM images of bare PP. b) EDS mapping images of CFP-PP. The breaks generated by plasma were enriched in O elements.

3. Rate Performance

With a fixed current density of 1 mA cm^{-2} and increasing the discharge capacity, CFP-PP exhibited a lower polarization than bare PP, and bare PP short-circuited when the discharge capacity reached 20 mAh cm^{-2}, while CFP-PP still cycled stably with an overpotential of only 46 mV.

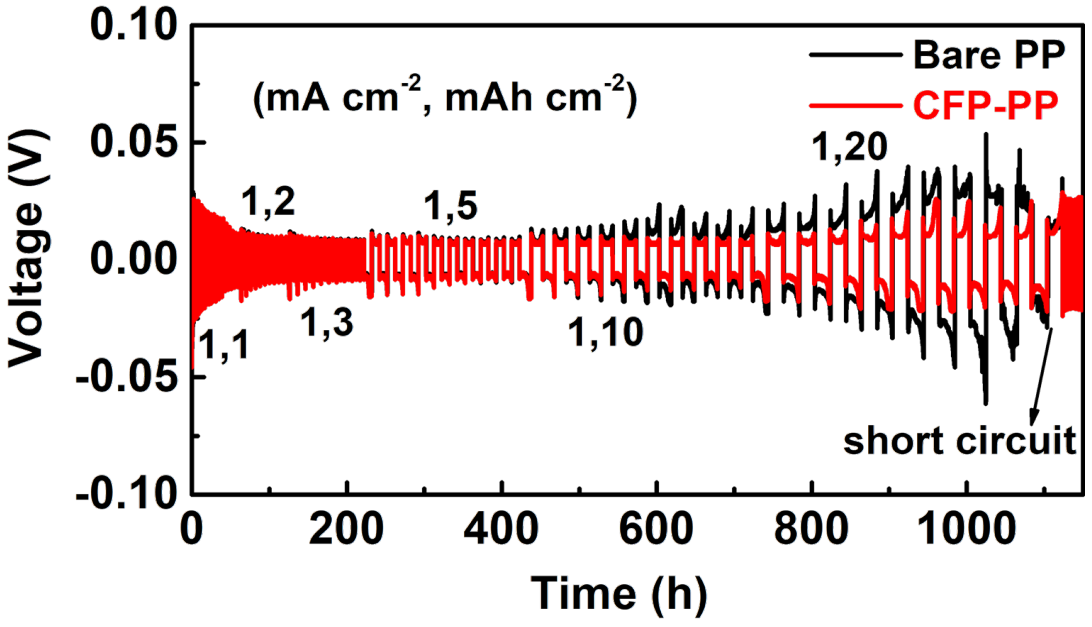

Fig. S3. Rate performance of bare PP and CFP-PP.

4. XPS Characterization

Table S1. Contents of F element in Li anodes and separators before and after cycles of bare PP and CFP-PP

Contents of F element/%	Li anode of bare PP	Li anode of CFP- PP	Separator of bare PP	Separator of CFP-PP
Before cycle			0	46.86
1 cycle	3.29	4.61	4.89	15.12
10 cycles	1.29	1.68	1.18	3.05
100 cycles	2.27	9.84	17.06	23.97

5. AFM Characterization

AFM reveals that the lithium anode using bare PP as the separator has a very rough surface and exhibits numerous protrusions after 10 and 100 cycles. The lithium anode equipped with CFP-PP separator, on the other hand, showed a comparatively flat and smooth shape, showing that CFP-PP is useful in preventing the production of lithium dendrites.

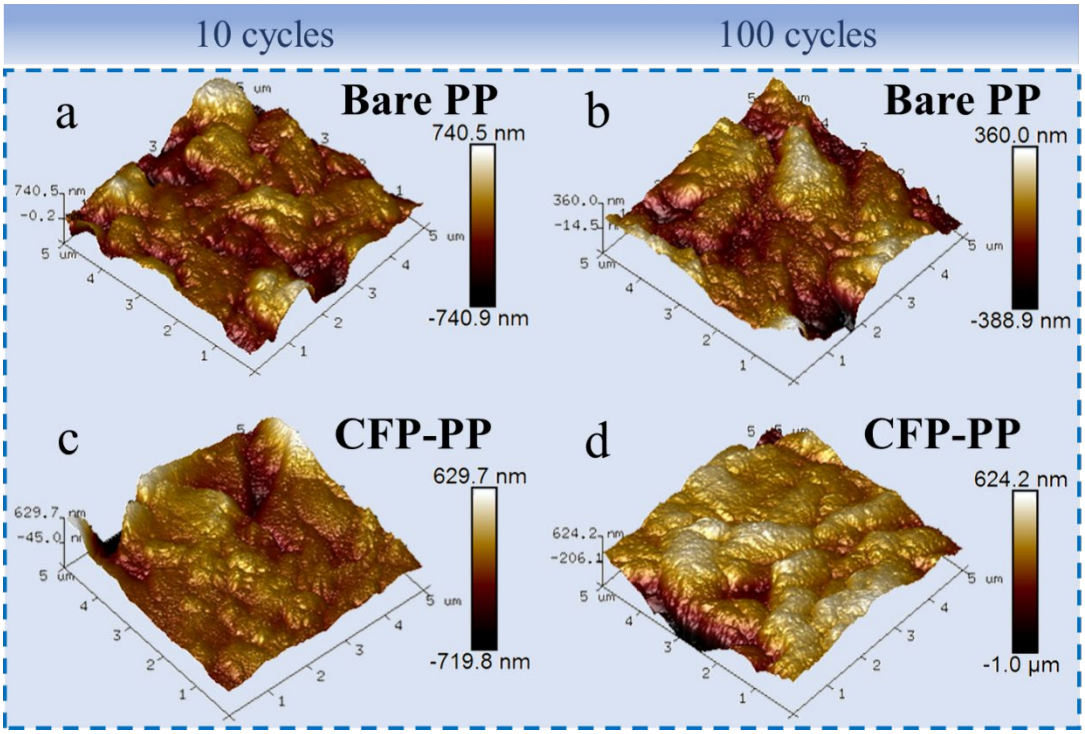

Fig. S4. AFM images of bare PP after a) 10 cycles, b) 100 cycles; AFM images of CFP-PP after c) 10 cycles, d) 100 cycles.

6. Li||LFP Full Cells

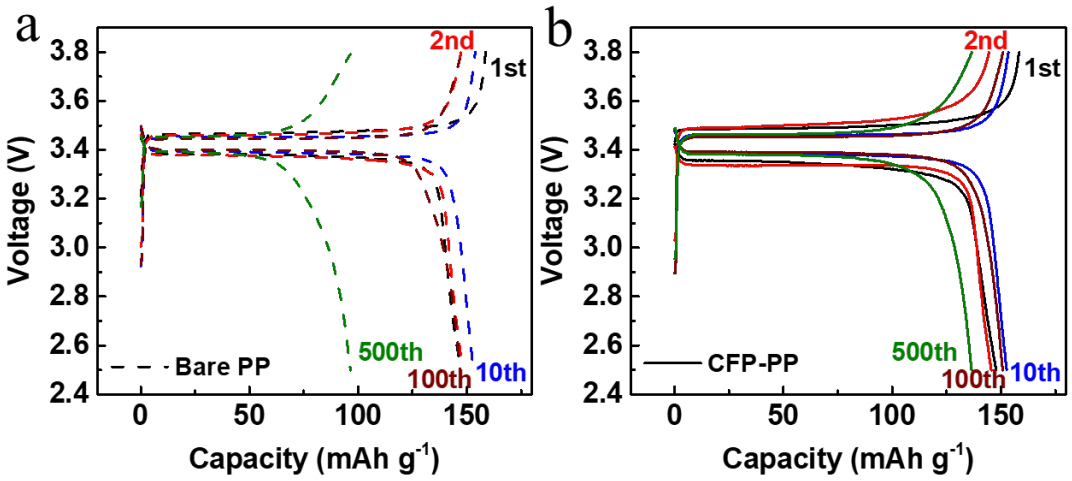

Fig. S5. Discharge curves of Li||LFP full cells equipped with a) bare PP, b) CFP-PP.

7. Li||LFP Full Cells

Li||LFP full cells were assembled in ester electrolyte (1M $LiPF_6$/EC-DEC). The full cell equipped with a CFP-PP separator displayed excellent cycling stability, with a capacity of 110.5 mAh g^{-1} after 200 cycles at 1C, corresponding to a capacity retention of 86.1 %. In contrast, the capacity of the full cell with bare PP was only 60.6 mAh g^{-1} with a capacity retention of 52.1 %.

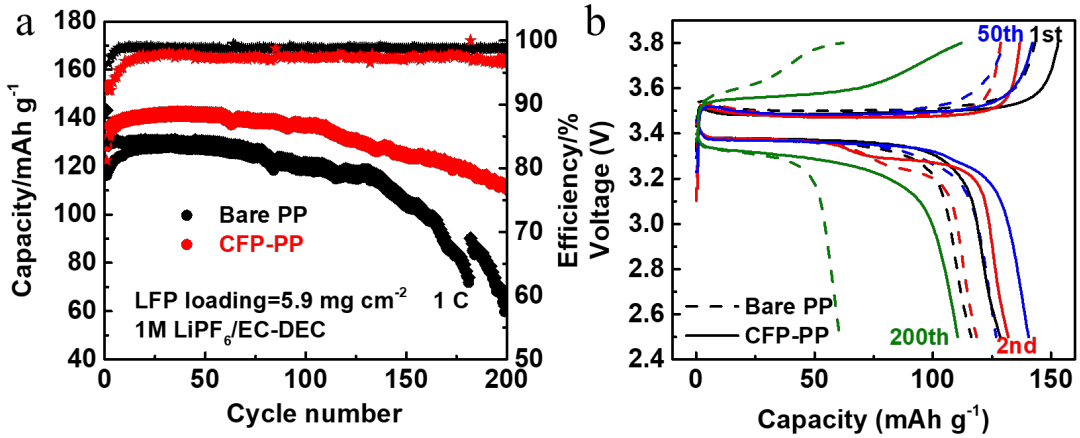

Fig. S6. a) Electrochemical performance and b) discharge curves of Li||LFP full cells equipped with bare PP and CFP-PP in 1M $LiPF_6$/EC-DEC.

8. XPS Characterization

To determine the impact of plasma parameter optimization on the amount of F on Polypropylene separator, three additional treatment parameters—CFP-PP-0.5, CFP-PP-2, and CFP-PP-80—were added. These parameters were adjusted the treatment time to 0.5 min and 2 min, increased the treatment power to 80 W, and left other parameters unchanged. The XPS test results showed that the three have F contents of 0.6%, 8.1%, and 42.2%, respectively.

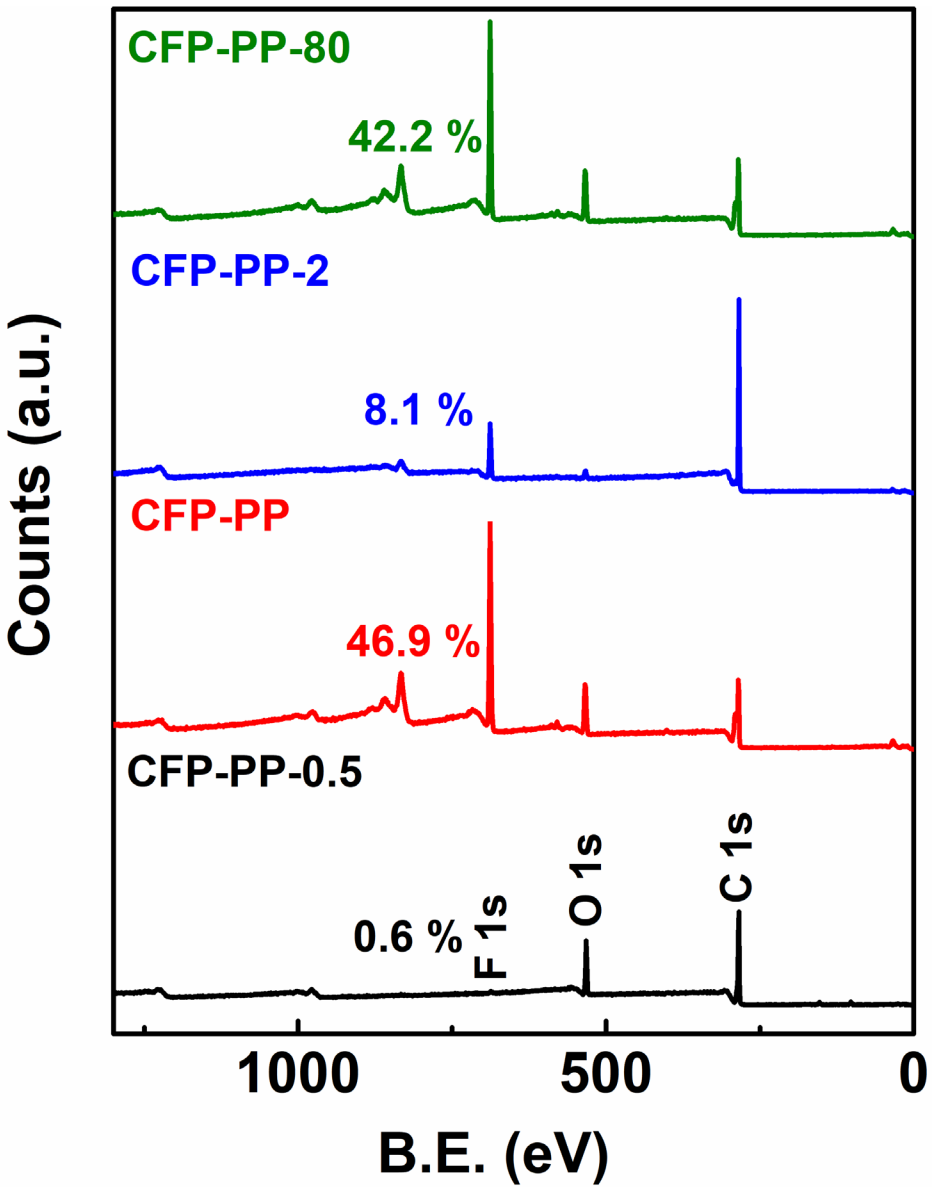

Fig. S7. XPS spectra of CFP-PP-0.5, CFP-PP, CFP-PP-2 and CFP-PP-80 separator

9. SEM Images

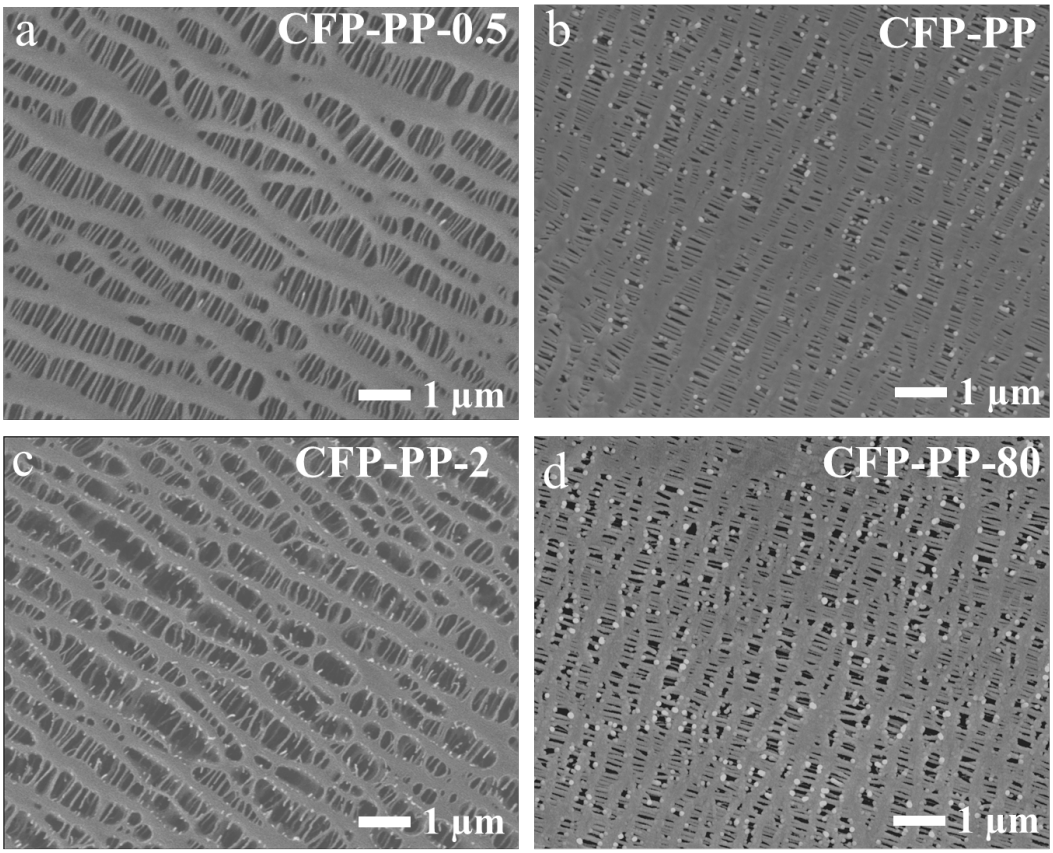

Fig. S8. SEM images of CFP-PP-0.5, CFP-PP, CFP-PP-2 and CFP-PP-80 separator

10. SEM Images

The surface morphology of the lithium foil after 10 cycles were shown in Fig S9. The lithium anode surface for the cell using the CFP-PP-0.5 separator exhibited a large agglomerated morphology with poor conductivity and dead lithium formation; the surface for the CFP-PP-2 separator had a similar morphology with CFP-PP-0.5, but the agglomerated particles were smaller in size; meanwhile, the lithium deposited on the surface of the CFP-PP-80 separator was distributed more uniformly but had a greater degree of agglomeration than the CFP-PP.

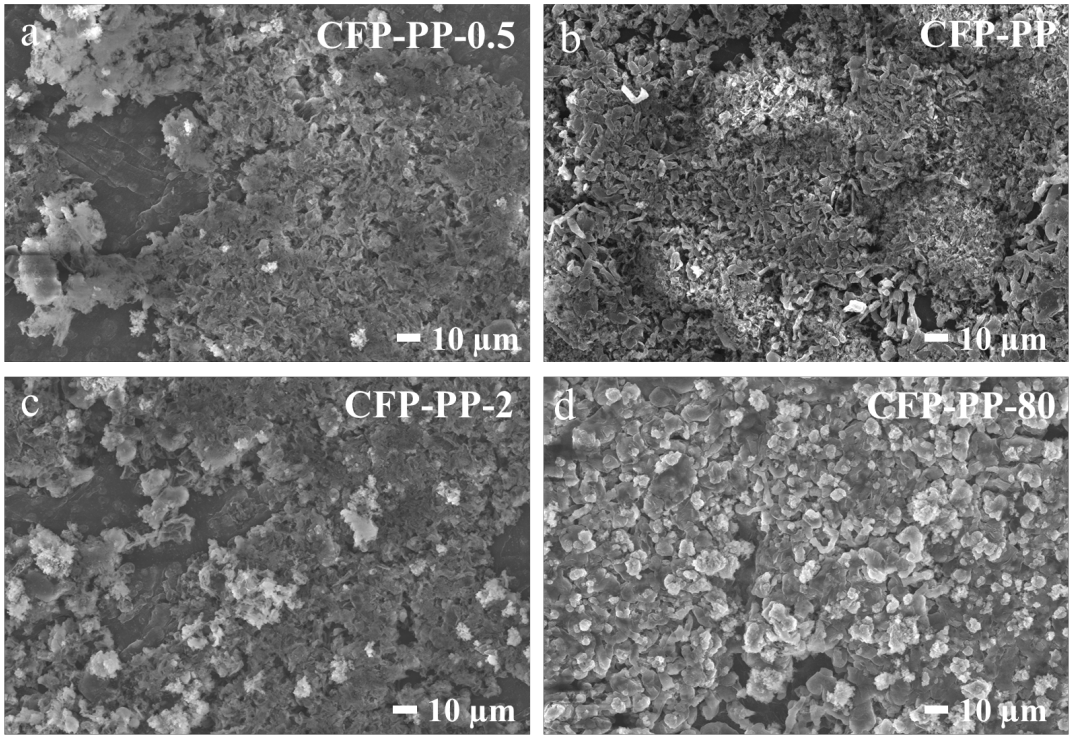

Fig. S9. Top-view SEM images of Li anodes equipped with a) CFP-PP-0.5, b) CFP-PP, c) CFP-PP-2 and d) CFP-PP-80 separator after 10 cycles

11. XPS Characterization

The primary impacts of various treatment parameters on the surface composition of lithium metal after cycling were identified by XPS testing. Using the CFP-PP-0.5 and CFP-PP-2 separators with lower F content results in a lithium anode with higher Li_2CO_3 concentration which suggests that these separators are less effective in inhibiting the electrolyte decomposition. The content of LiF is less affected, though.

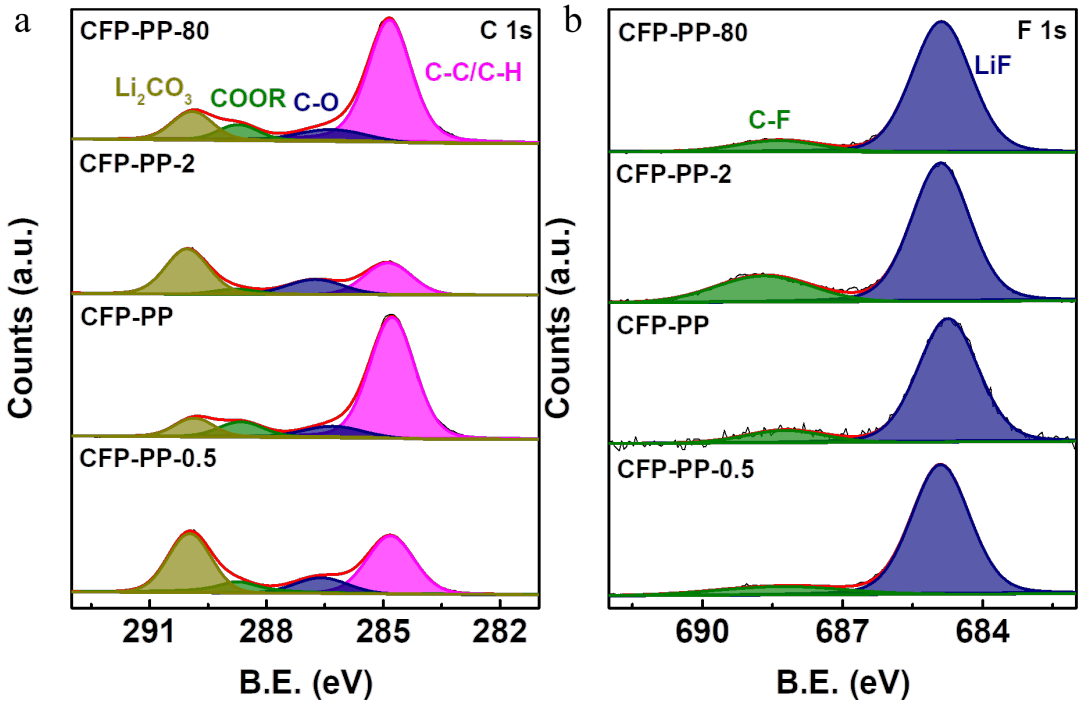

Fig. S10. XPS spectra for a) carbon 1s, b) fluorine 1s of Li anode with CFP-PP-0.5, CFP-PP, CFP-PP-2 and CFP-PP-80 separator after 10 cycles

12. SEM Image and Elemental Mapping Images

As shown in the XPS characterization, a weak O1s peak was observed in the PP separator after CF_4 treatment, which might be due to the introduction of oxygen-containing functional groups when the highly activated PP was exposed to air after plasma treatment. To characterize the role of oxygen-containing functional groups, the PP separator was treated with a feed gas of a mix of CF_4 and O_2 gas (flow rate = 3:1). CFOP-PP represented similar breaks enriched in O elements as CFP-PP.

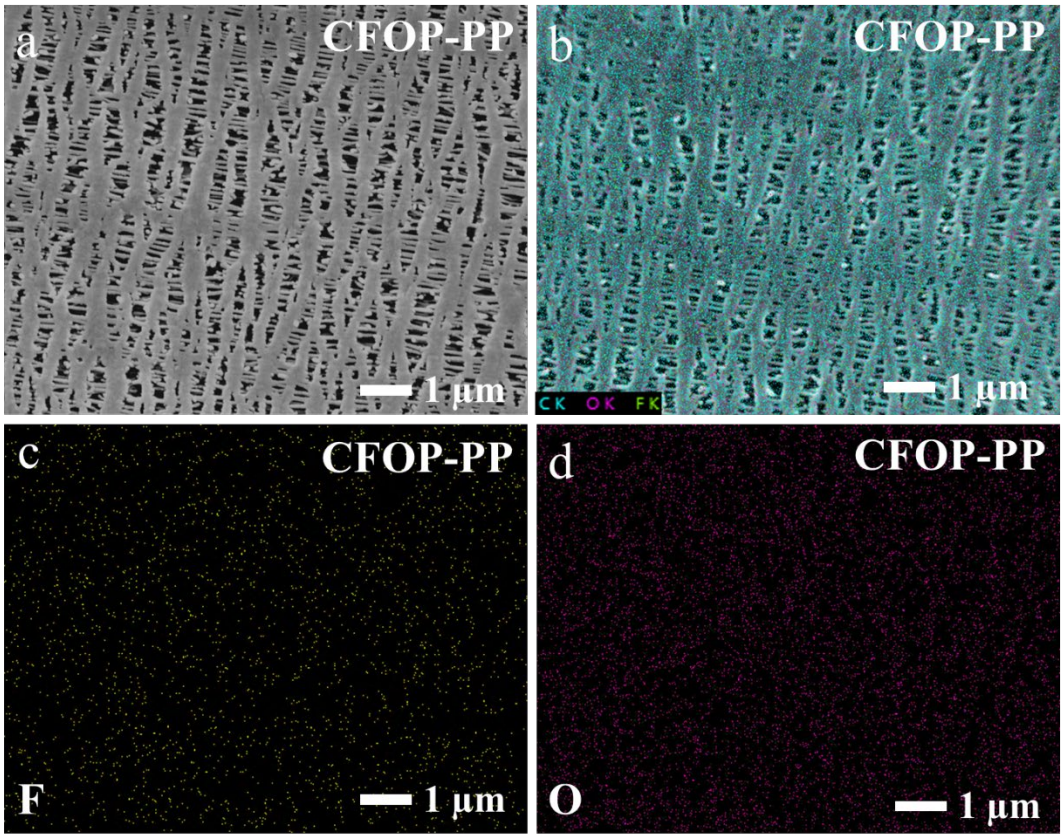

Fig. S11. a) SEM image, b) EDS elemental map, c) fluorine EDS elemental map, d) oxygen EDS elemental map of CFOP-PP.

13. FTIR Spectra

The FTIR spectra of CFOP-PP were the same as CFP-PP, with broad peaks of -OH stretching at 3650-3200 cm^{-1} and C=O and CF_2 stretching at 1715 cm^{-1} and 1167 cm^{-1}, respectively.

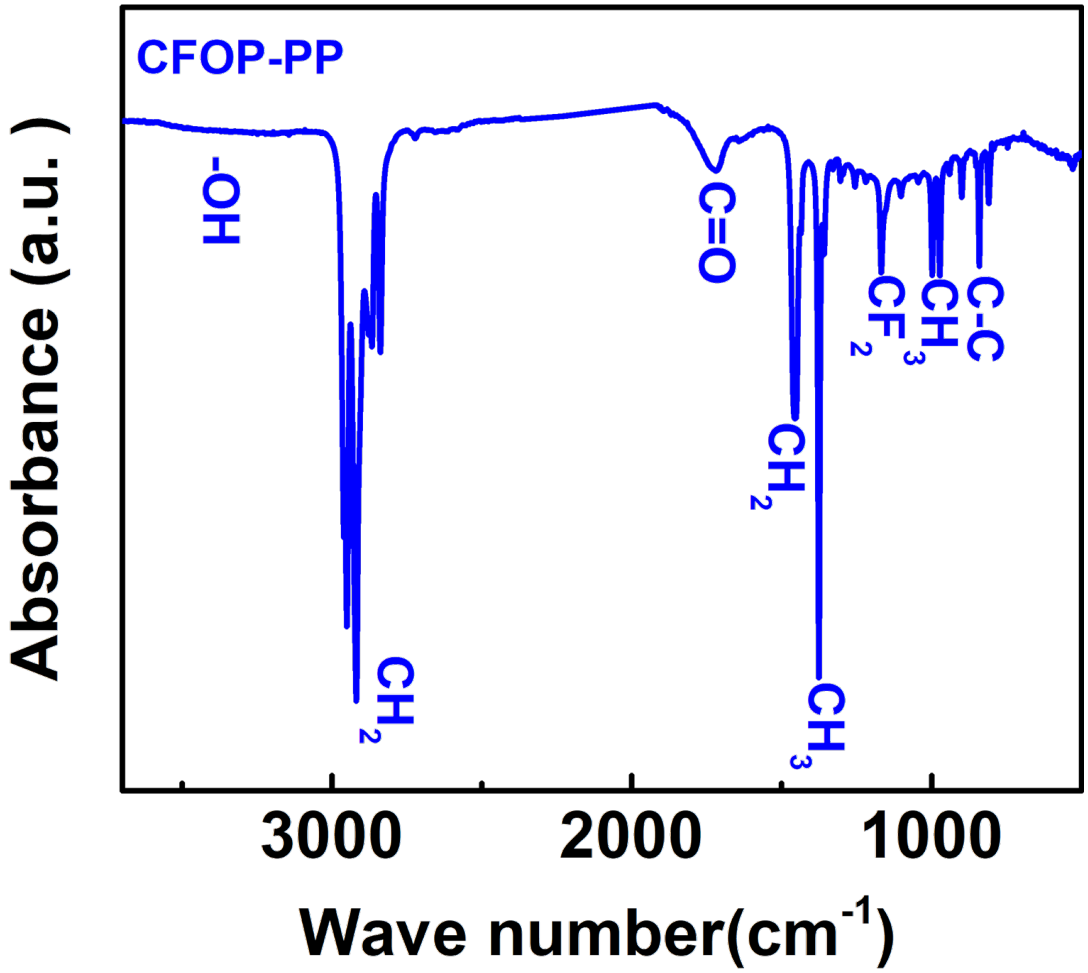

Fig. S12. Fourier transform infrared spectrometer (FTIR) spectra of CFOP-PP.

14. XPS Spectra

XPS spectra of CFOP-PP showed that the molar contents of C, O, and F elements were 81.4%, 14.2%, and 4.4%, respectively. Compared with CFP-PP, CFOP-PP exhibited a higher content of O elements, indicating that the mixed O_2 gas provided more oxygen-containing functional groups. Moreover, the contents of functional groups were particularly different between CFP-PP and CFOP-PP. In the O1s peak, CFOP-PP showed higher -OH and C=O contents but lower C-O-C content than CFP-PP, and in the F1s peak, higher semi-ionic C-F bonds and lower covalent C-F bonds were exhibited in CFOP-PP, while the CF_x even disappeared. This indicated that the introduction of O_2 feed gas not only changed the composition of the oxygen-containing functional groups but also influenced the fluorine-containing functional groups.

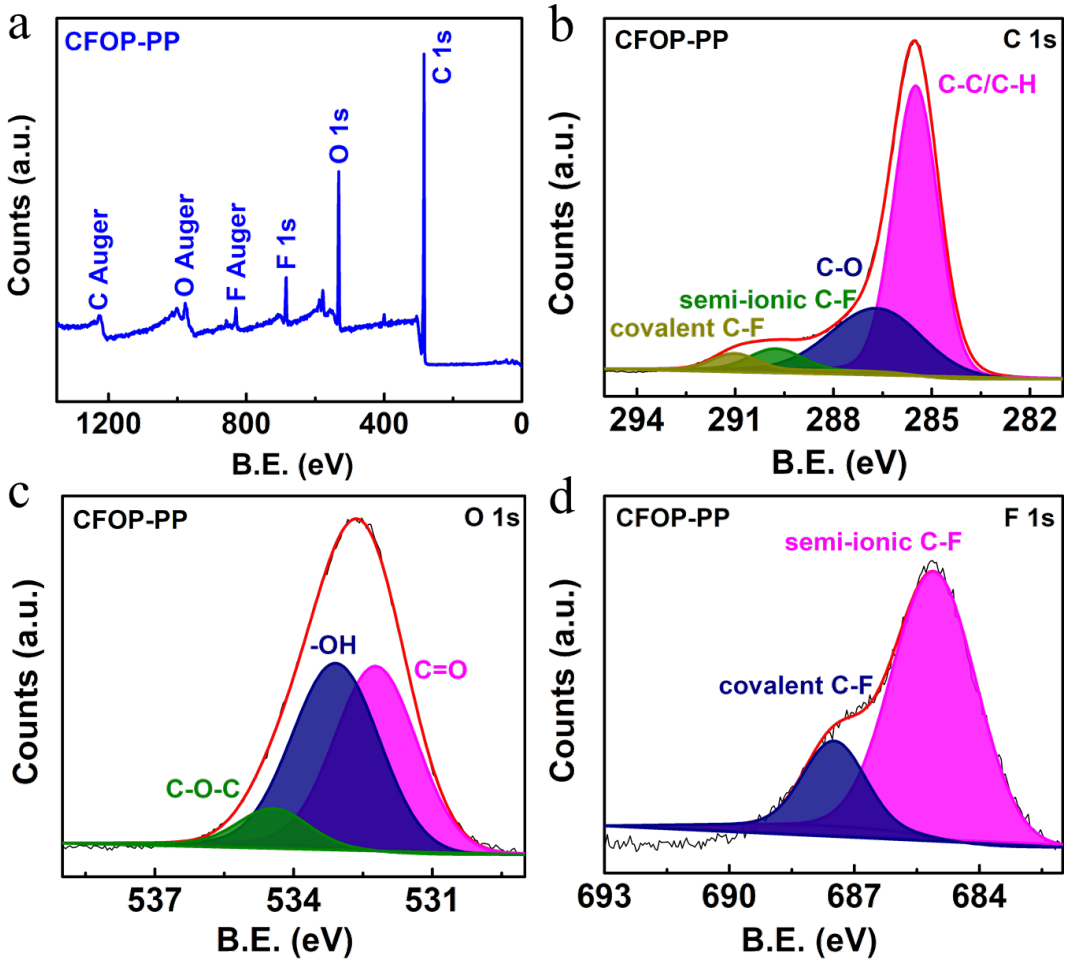

Fig. S13. a) X-ray photoelectron spectroscopy (XPS) spectra, b) XPS spectra for carbon 1s, c) oxygen 1s, h) fluorine 1s of CFOP-PP.

15. Contact Angle

The contact angle of the electrolyte on CFOP-PP was 28.3°, which is smaller than bare PP but larger than CFP-PP.

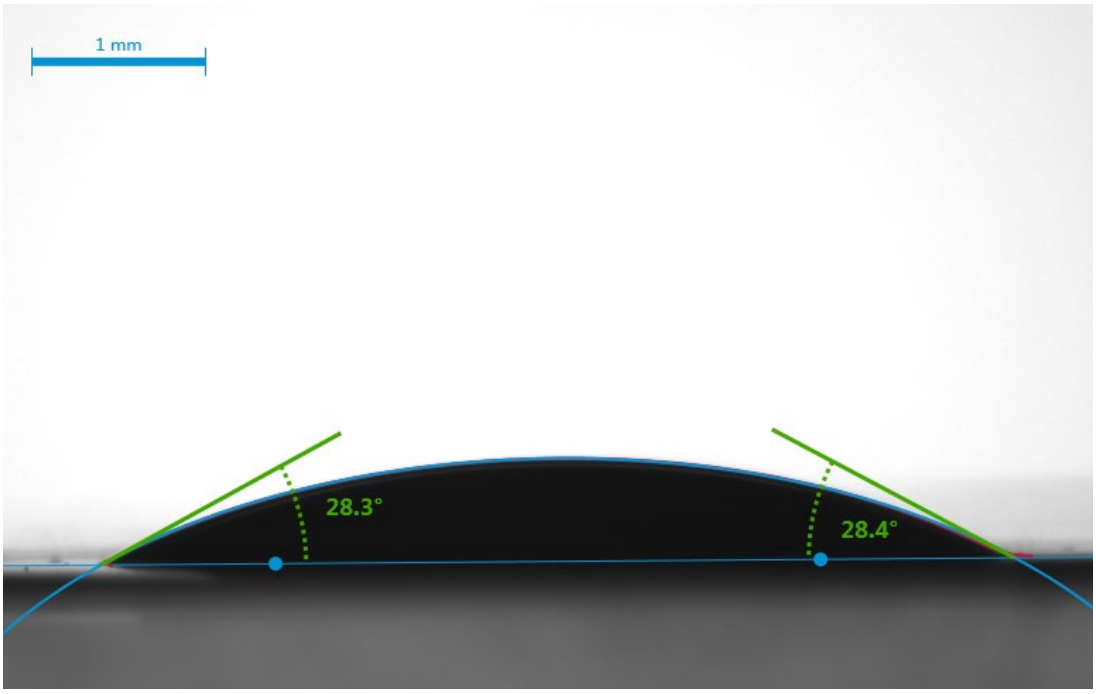

Fig. S14. Contact angle measurements of CFOP-PP.

16. Ionic conductivity

CFOP-PP showed a good lithium-ion conductivity (0.71 S cm^{-1}), which was nearly three times higher than bare PP (0.26 S cm^{-1}) but was smaller than CFP-PP.

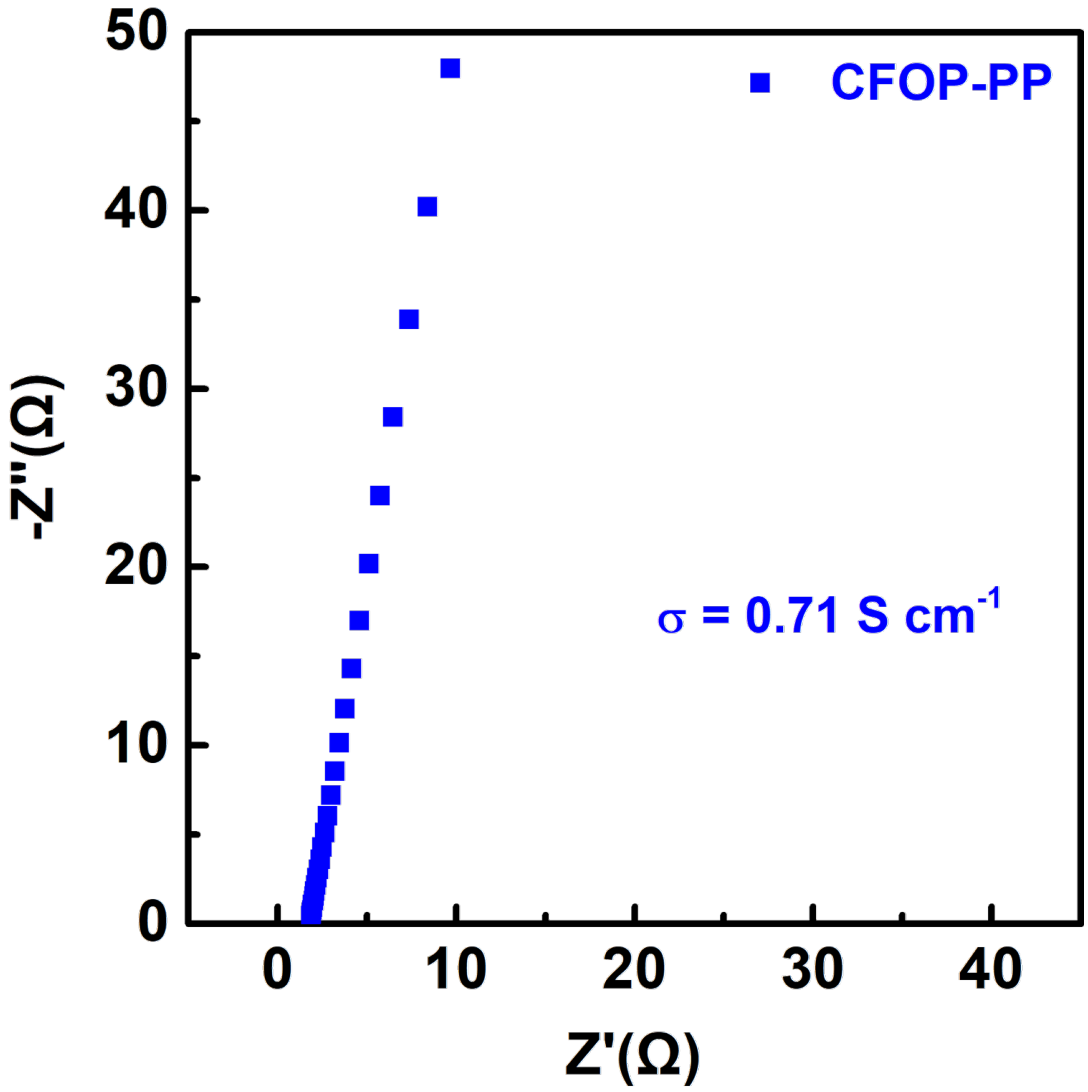

Fig. S15. Ionic conductivity of CFOP-PP.

17. Lithium-Ion Transference Number

The Li^+ transference number of CFOP-PP was 0.43, which was higher than bare PP (t_{Li+} = 0.36) but was smaller than CFP-PP (t_{Li+} = 0.65).

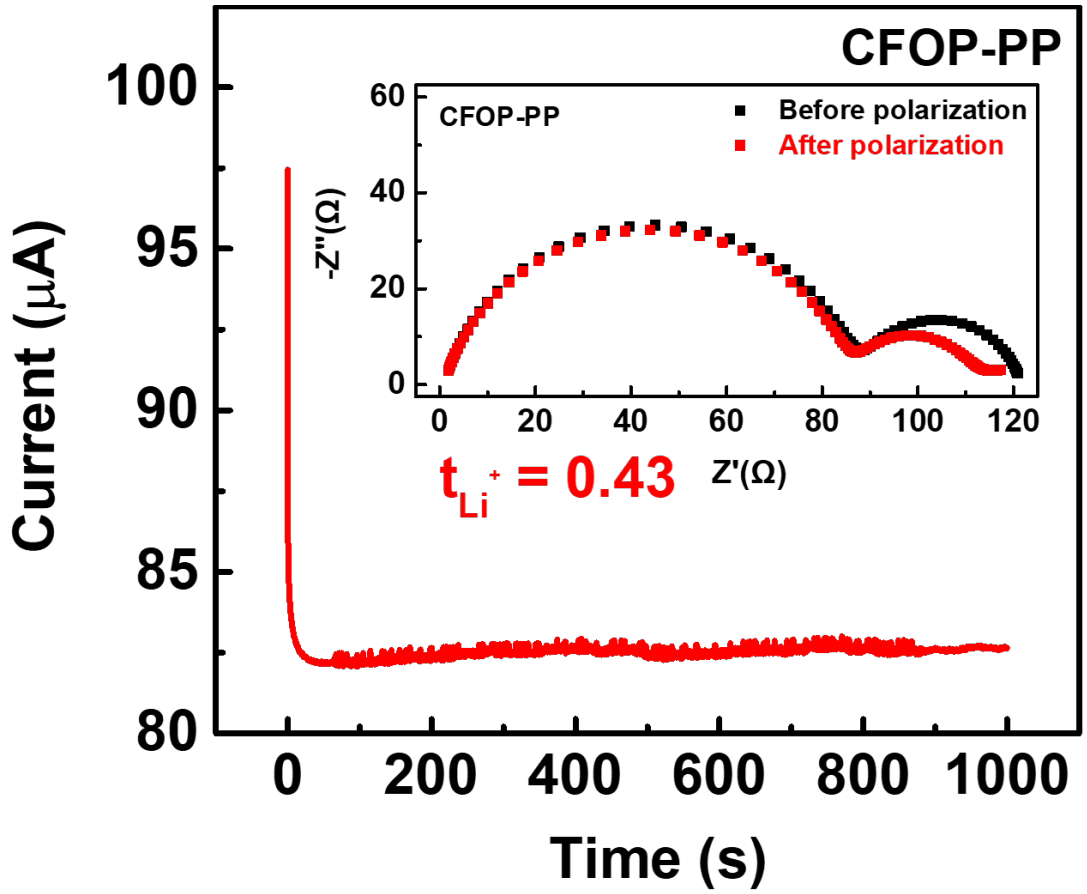

Fig. S16. Chronoamperometry profiles of CFOP-PP separators under an initial bias voltage of 10 mV (The inset shows the corresponding EIS results of Li||Li symmetrical cells before and after chronoamperometry).

18. Electrochemical Performance of Li||Li Symmetric Cell

the symmetric cell equipped with a CFOP-PP separator presented an overpotential of 162 mV at a current density of 1 mA cm^{-2} and an areal capacity of 1 mAh cm^{-2} and short-circuited after 4380 h, which represented a higher overpotential and a shorter cycle performance than CFP-PP, indicating the improvement of fluorine-containing functional groups on separator was better than the oxygen-containing functional groups.

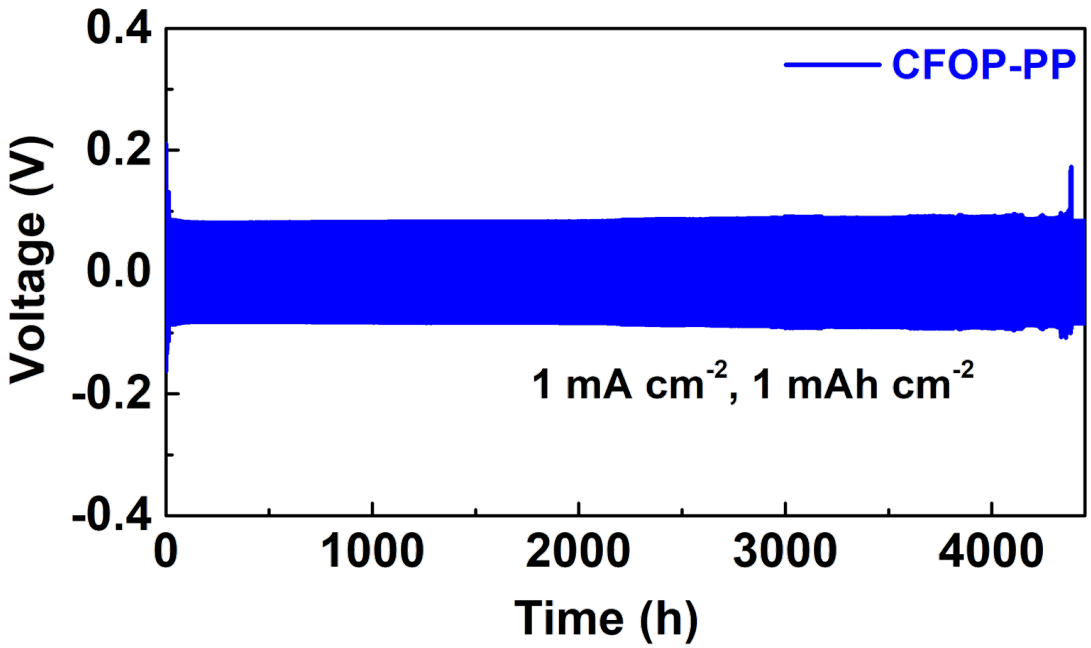

Fig. S17. Electrochemical performance of Li||Li symmetric cells with CFOP-PP at the current density of 1 mA cm^{-2} and capacity of 1 mAh cm^{-2}.

19. Electrochemical Impedance Spectra

Table S2. Electrochemical impedance fitted data for symmetric cells of bare PP and CFP-PP

Before cycle

Sample	R_{ct} [Ω]
Bare PP	202.8
CFP-PP	9.8

10 cycles

Sample	R_{SEI} [Ω]	R_{ct} [Ω]
Bare PP	24.2	59.4
CFP-Li-20	5.9	12.6

100 cycles

Sample	R_{SEI} [Ω]	R_{ct} [Ω]
Bare Li	4.7	19.9
CFP-Li-20	1.2	11.7

20. XPS spectra

For bare PP, low contents of F elements appeared after 1, 10, and 100 cycles. The few F contents might be derived from the decomposition of the electrolyte.

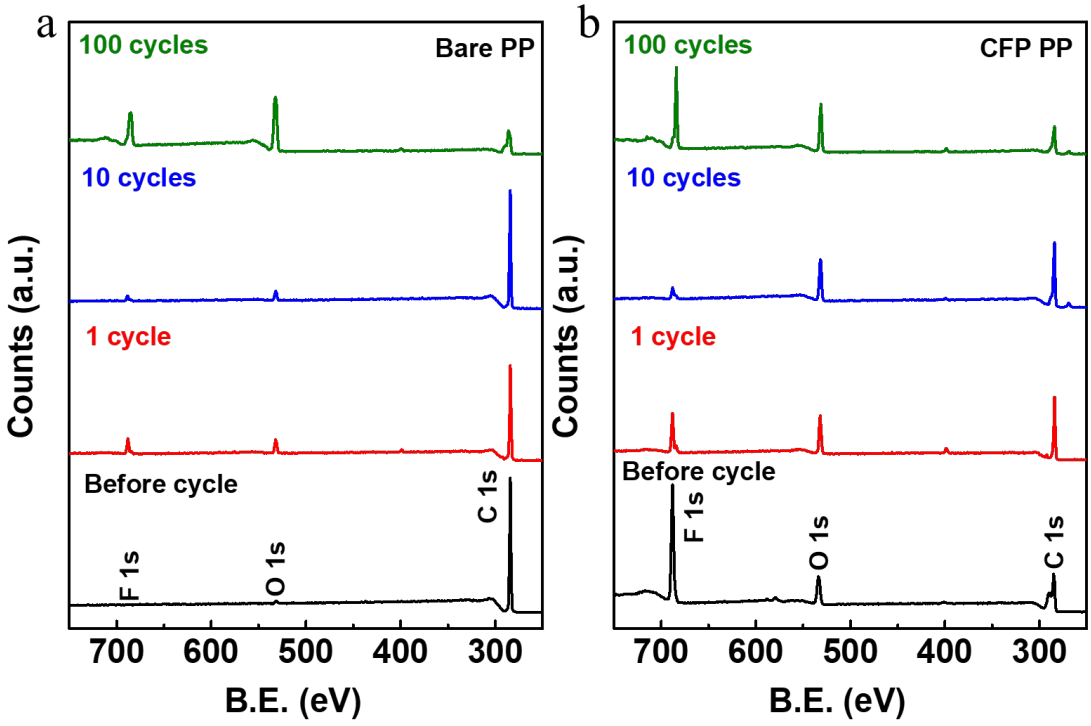

Fig. S18. a) XPS spectra of bare PP separator; b) CFP-PP separator.

21. SEM Images

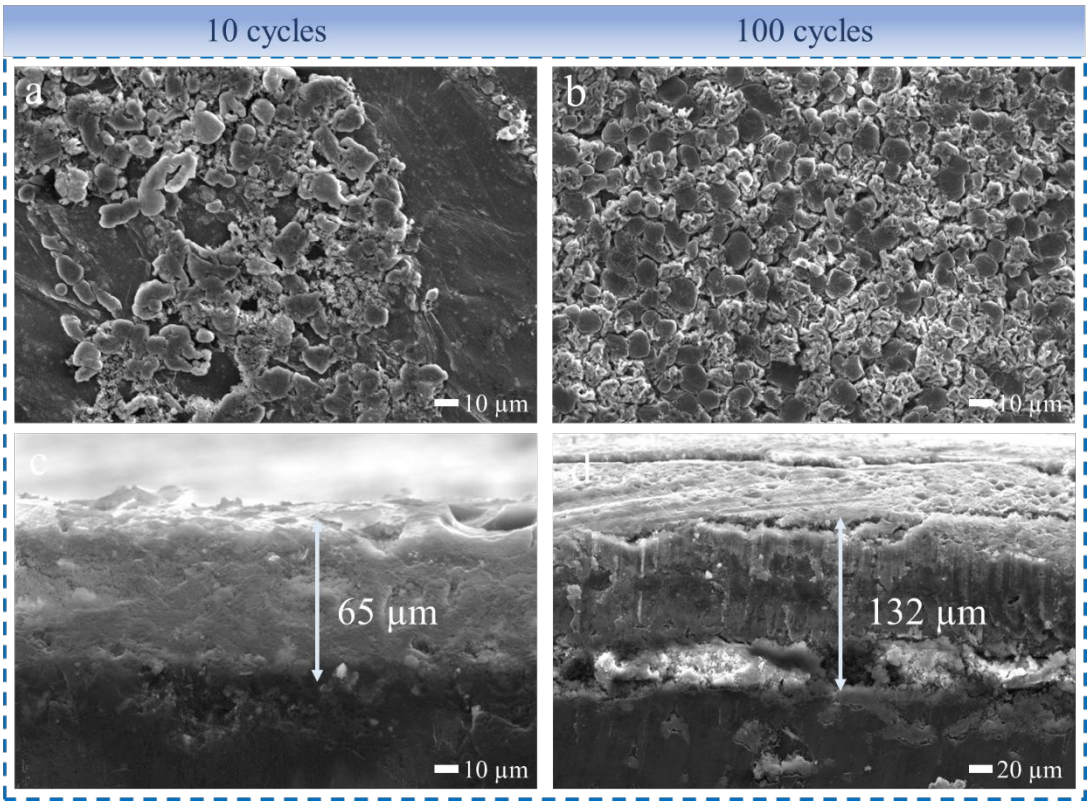

Fig. S19. Top-view SEM images of CFOP-PP after a) 10 cycles, b) 100 cycles; cross-sectional SEM images of CFOP-PP after c) 10 cycles, d) 100 cycles.

22. Optical Photos of Li Metal Anodes

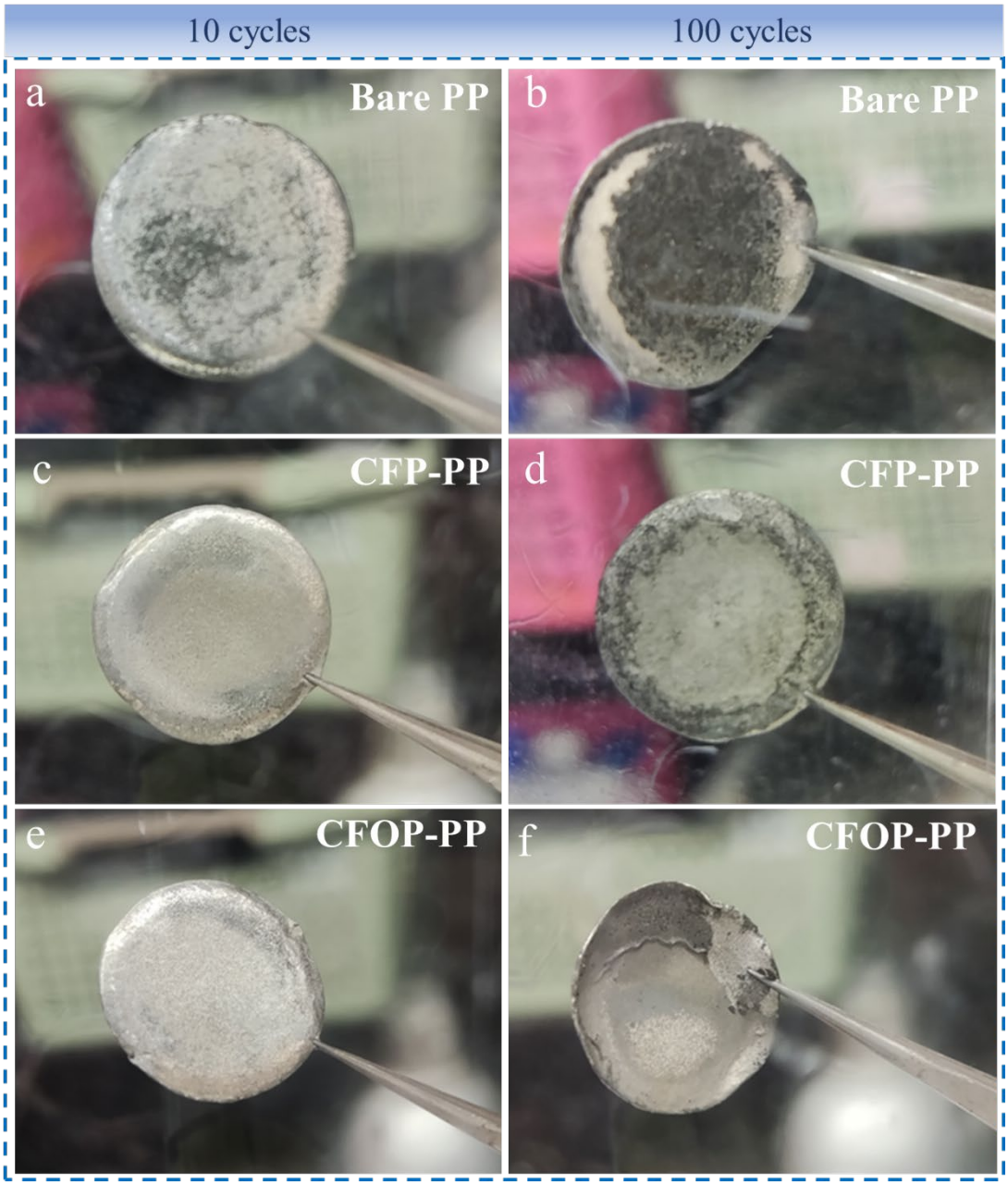

Fig. S20. Optical photo of Li metal anodes with bare PP separator after a) 10 cycles, b) 100 cycles; CFP-PP separator after c) 10 cycles, d) 100 cycles; CFOP-PP separator after e) 10 cycles, f) 100 cycles.

23. Optical Photos of PP Separators

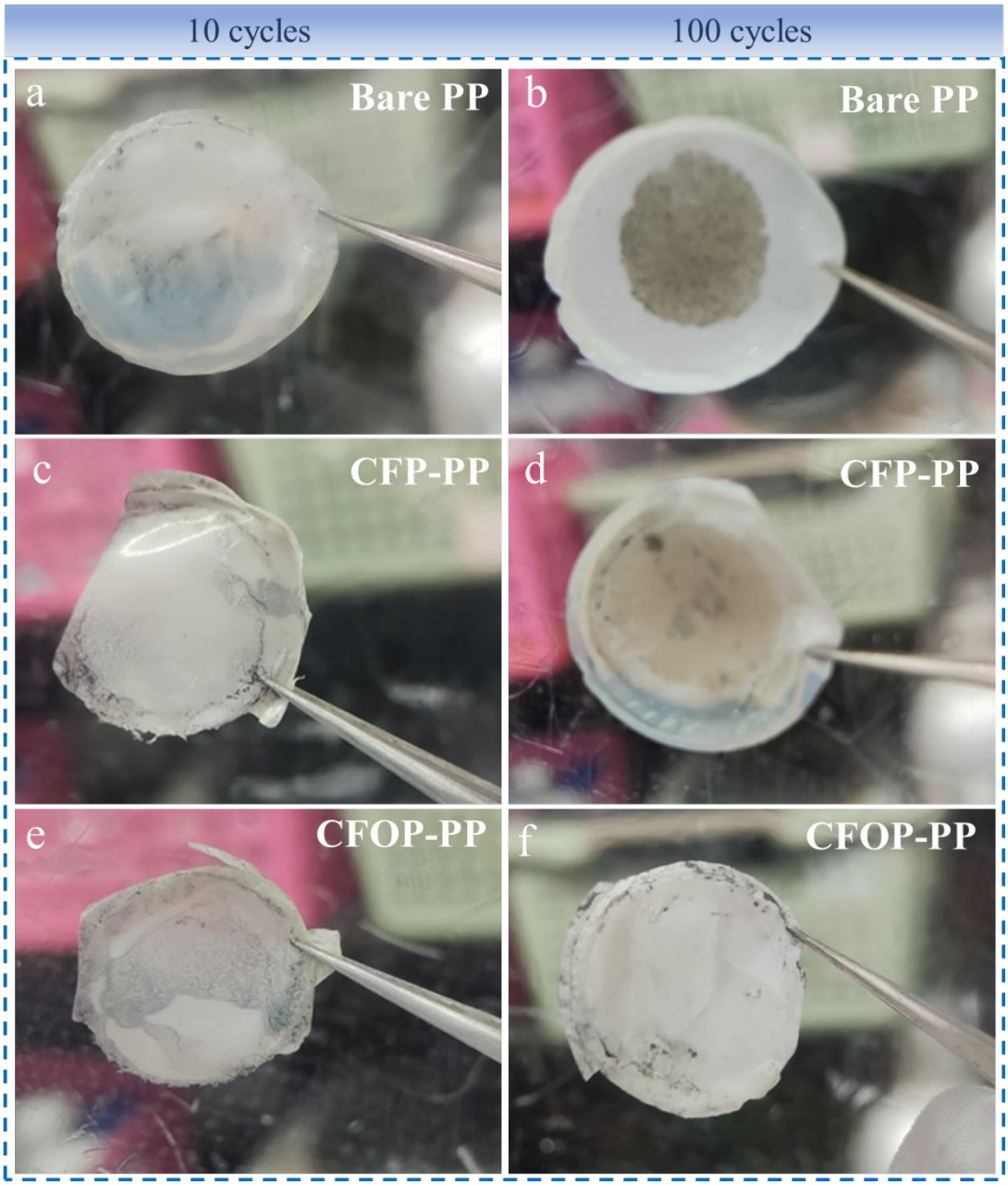

Fig. S21. Optical photo of bare PP separator after a) 10 cycles, b) 100 cycles; CFP-PP separator after c) 10 cycles, d) 100 cycles; CFOP-PP separator after e) 10 cycles, f) 100 cycles.

24. SEM-EDS Line Scan Analysis

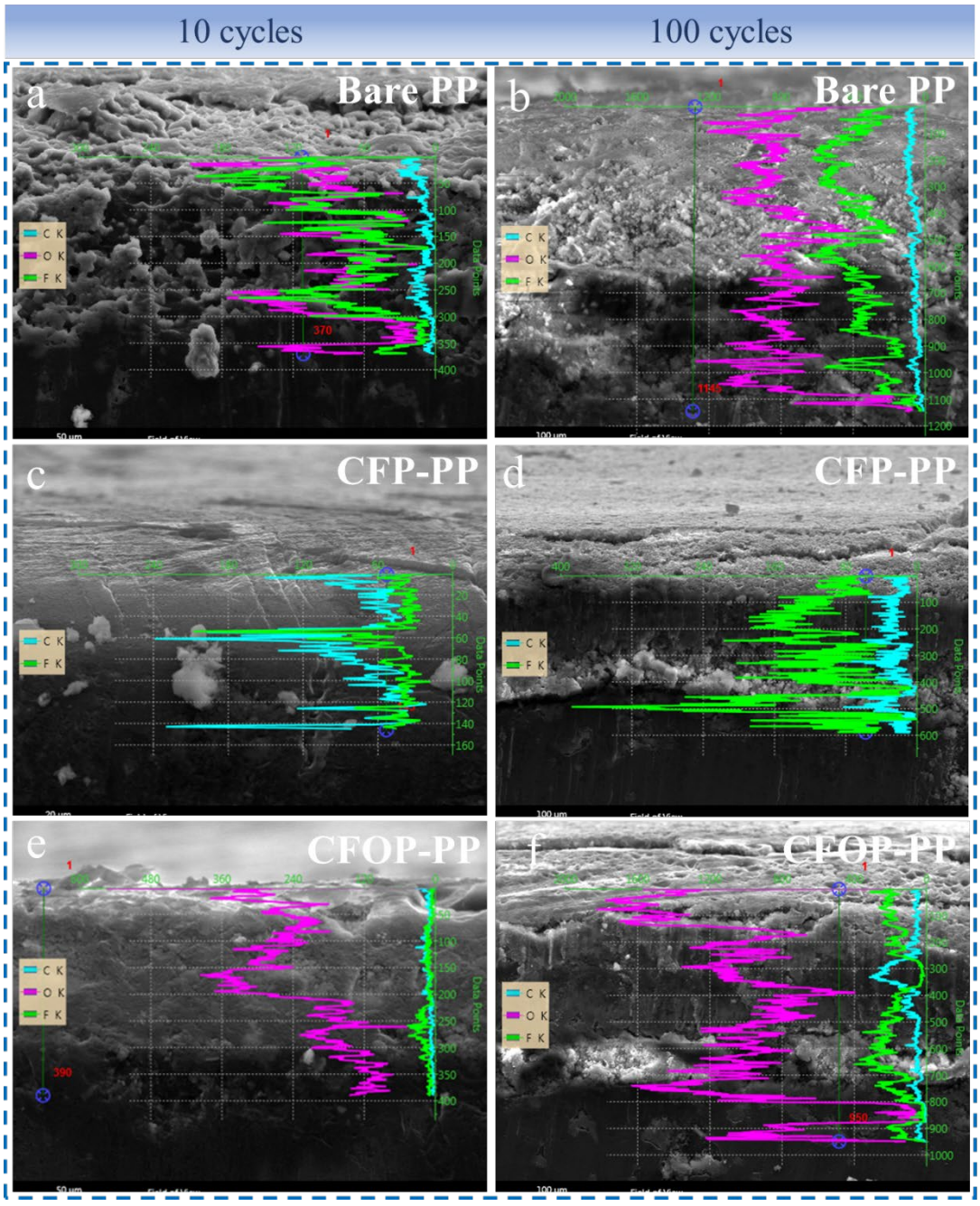

Fig. S22. SEM-EDS line scan analysis of Li metal anodes with bare PP separator after a) 10 cycles, b) 100 cycles; CFP-PP separator after c) 10 cycles, d) 100 cycles; CFOP-PP separator after e) 10 cycles, f) 100 cycles.

25. SEM Images

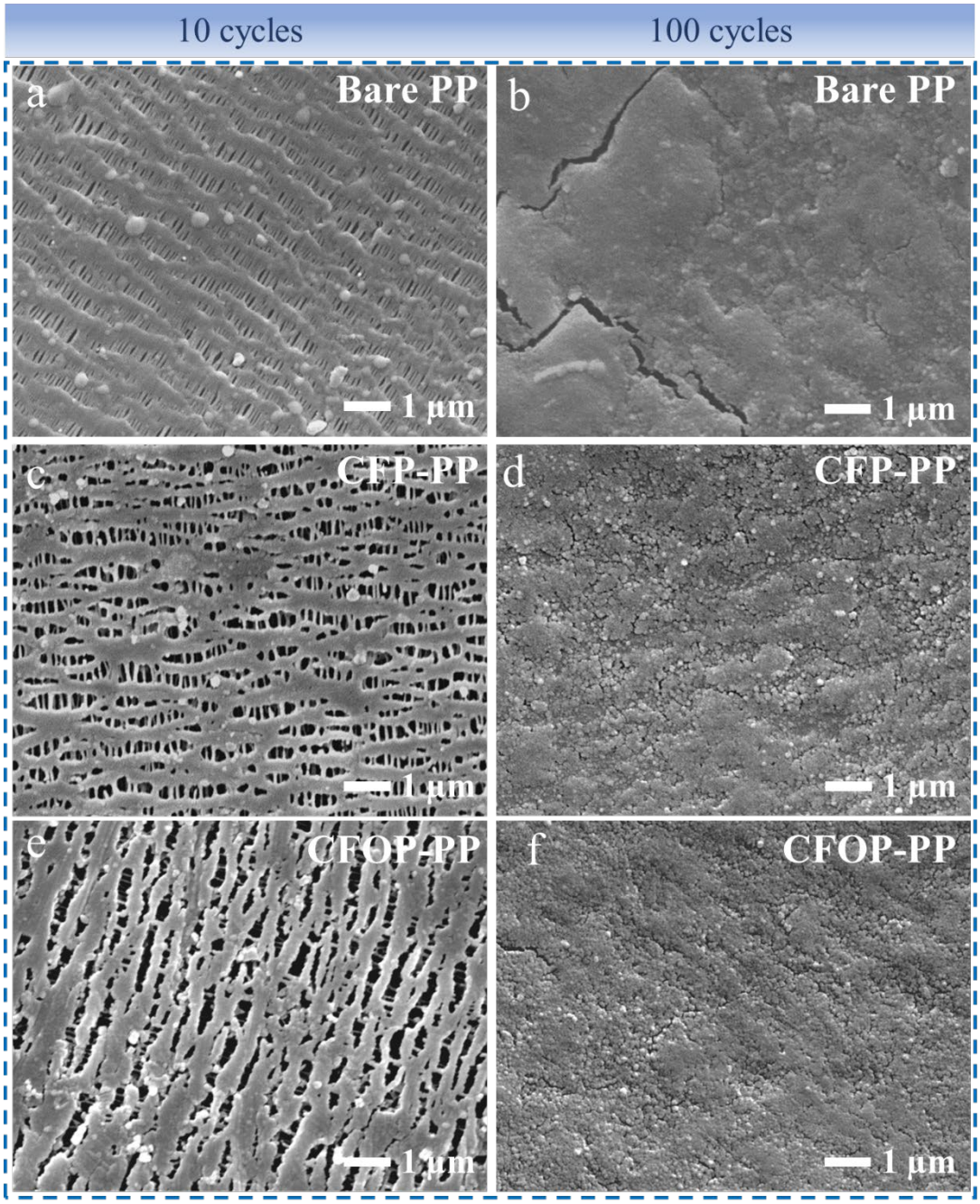

Fig. S23. SEM images of bare PP separator after a) 10 cycles, b) 100 cycles; CFP-PP separator after c) 10 cycles, d) 100 cycles; CFOP-PP separator after e) 10 cycles, f) 100 cycles.

26. Electrochemical Performance of Li||Cu Half Cell

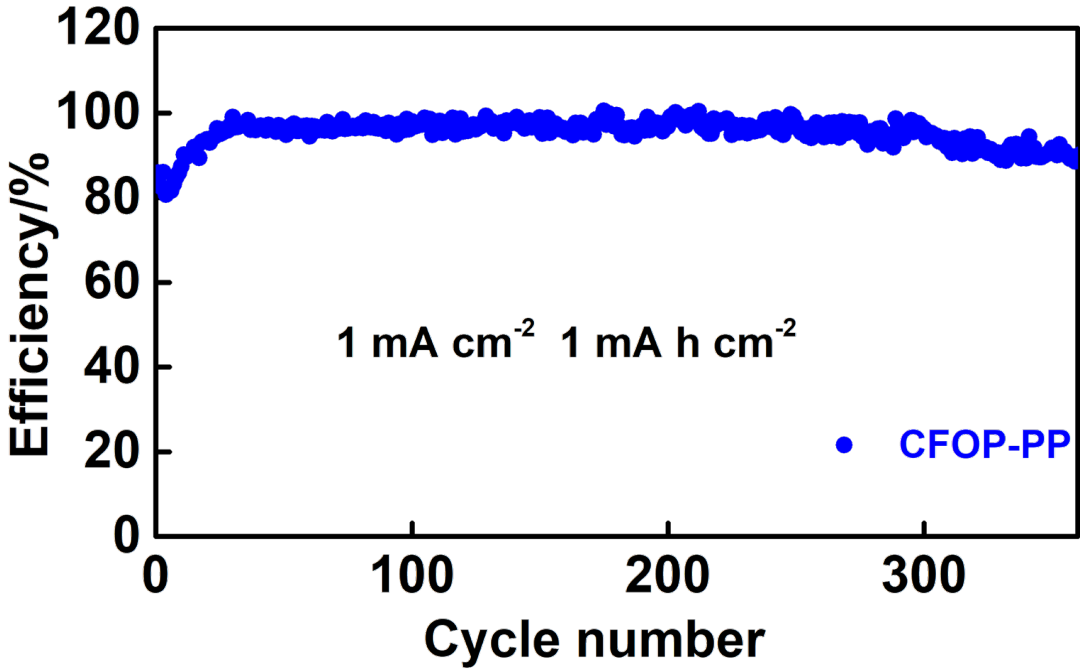

Fig. S24. Electrochemical performance of Li||Cu half cells with CFOP-PP at 1 mA cm^{-2} and 1 mAh cm^{-2}.

27. XPS Spectra

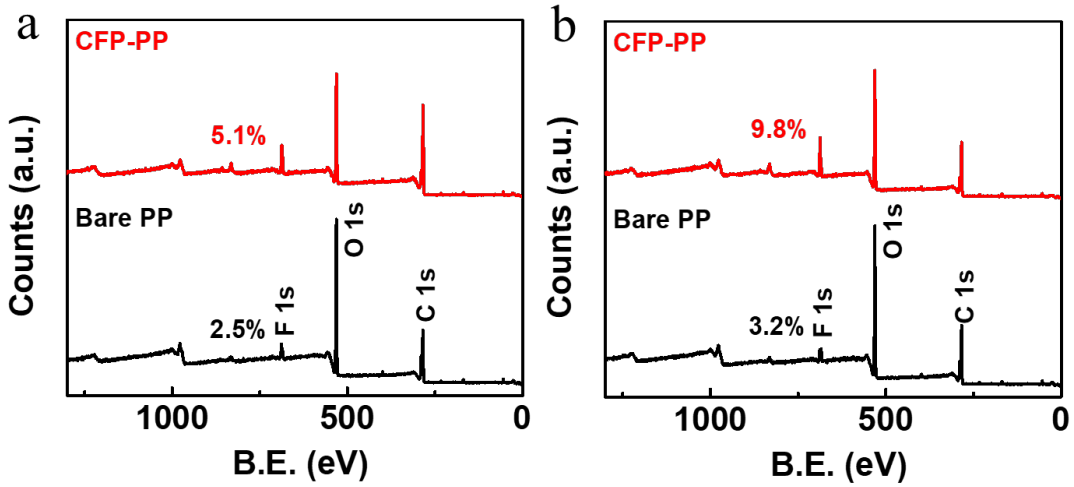

Fig. S25. a) XPS spectra of graphene anodes equipped with CFP-PP and bare PP after 1 cycle, b) after 10 cycles.

28. The Li||Li Symmetric Cells in Literature

Table S3. The summary of cycle performance of Li||Li symmetric cells in the literature

Method	Electrolyte	Current density (mA cm^{-2})	Capacity (mAh cm^{-2})	Lifespan (h)	Ref.
Fluorine-containing groups grafted PP separator	LiTFSI+DOL/DME+1% LiNO3	1	1	7000	This work
Fe3N@N-doped graphene/PP	LiTFSI+DOL/DME+1% LiNO3	2	1	2000	[1]
COF/PVDF separator	LiPF6+EC/EMC	1	1	700	[2]
bicomponent core-shell structured polymeric separator	LiPF6+EC/DEC +10% FEC	1	1	1000	[3]
[Al2O3-OOC(CH2)2X] coated PP separator	LiTFSI+DOL/DME+1% LiNO3	1	1	2500	[4]
COF-COOH@PP separator	LiTFSI+DOL/DME+5% LiNO3	1	1	1100	[5]
Functional separator	LiTFSI+DOL/D	1	1	500	[6]

ME+2% LiNO3

References

1. X. Zhang, F. Ma, K. Srinivas, B. Yu, X. Chen, B. Wang, X. Wang, D. Liu, Z. Zhang, J. He and Y. Chen, *Energy Stor. Mater.*, 2022, **45**, 656-666.
2. Y. Yang, S. Yao, Z. Liang, Y. Wen, Z. Liu, Y. Wu, J. Liu and M. Zhu, *ACS Energy Lett.*, 2022, **7**, 885-896.
3. J. Ryu, D.-Y. Han, D. Hong and S. Park, *Energy Stor. Mater.*, 2022, **45**, 941-951.
4. Y. Liu, X. Tao, Y. Wang, C. Jiang, C. Ma, O. Sheng, G. Lu and X. W. D. Lou, *Science*, 2022, **375**, 739-745.
5. Q. An, H. e. Wang, G. Zhao, S. Wang, L. Xu, H. Wang, Y. Fu and H. Guo, *Energy & Environ. Mater.*, 2022, DOI: 10.1002/eem2.12345.
6. J. Liu, R. Xu, C. Yan, H. Yuan, J.-F. Ding, Y. Xiao, T.-Q. Yuan and J.-Q. Huang, *Energy Stor. Mater.*, 2020, **30**, 27-33.